Research Square

Preprints are preliminary reports that have not undergone peer review.
They should not be considered conclusive, used to inform clinical practice,
or referenced by the media as validated information.

Functional characterization of b4galt2 reveals distinct effects during infection with two grass carp reovirus strains of different genotypes

Xijuan Gao
Shanghai Ocean University
Chenyang Zhang
Shanghai Ocean University
Chendong Tao
Shanghai Ocean University
Xiaoxiao Chen
Shanghai Ocean University
Yingen Dai
Jiangxi Provincial Aquatic Biology Protection and Rescue Center
Jiale Li
Shanghai Ocean University
Yubang Shen
ybshen@shou.edu.cn
Shanghai Ocean University
Shumei Du
Nanchang Academy of Agricultural Sciences

Research Article

Keywords: grass carp, b4galt2, grass carp reovirus, host–virus interaction, glycosylation

Posted Date: November 23rd, 2026

DOI: https://doi.org/10.21203/rs.3.rs-11643008/v1

License: This work is licensed under a Creative Commons Attribution 4.0 International License.
Read Full License

Additional Declarations: No competing interests reported.

Abstract

Background

Grass carp (*Ctenopharyngodon idella*) is threatened by grass carp reovirus (GCRV). The glycosyltransferase gene *b4galt2* was previously identified as a candidate associated with GCRV resistance, but its role during infection remains unclear.

Methods and results

We characterized grass carp *b4galt2*, examined its expression in nine tissues from healthy fish (n = 3) and after GCRV-AH528 challenge (n = 3 fish per sampling time), and evaluated *b4galt2* overexpression in CIK cells infected with GCRV-JX01 (genotype I) or GCRV-AH528 (genotype II). The 1140-bp coding sequence encoded a 379-amino-acid protein with conserved galactosyltransferase domains, and B4galt2 was highly conserved among teleosts. *b4galt2* was expressed in all nine tissues, most strongly in the brain. Following challenge, expression changed early in muscle and heart and increased later in several immune-related tissues. In transiently transfected CIK cells, B4galt2-EGFP fluorescence was observed in nuclear and cytoplasmic regions. Compared with parental cells, stable *b4galt2*-overexpressing cells showed lower S9 transcript abundance and higher CCK-8–assessed viability at 48 h, together with less extensive plaque formation, during JX01 infection. During AH528 infection, S6 transcript abundance was higher at 24, 48, 72, and 96 h, whereas CCK-8–assessed viability was lower at 48 h.

Conclusions

b4galt2 showed tissue-dependent responses to GCRV challenge, and its overexpression was associated with contrasting cellular phenotypes during JX01 and AH528 infection, supporting its involvement in grass carp–GCRV interactions.

1. Introduction

Grass carp (*Ctenopharyngodon idella*) is one of the most important freshwater aquaculture species worldwide and is widely cultured for food production [1]. However, the sustainable development of grass carp aquaculture is severely threatened by infectious diseases, among which grass carp hemorrhagic disease caused by grass carp reovirus (GCRV) is one of the most serious viral diseases [2, 3]. GCRV infection can cause pronounced hemorrhagic signs and high mortality, particularly in juvenile grass carp, resulting in substantial losses to the aquaculture industry [2, 4]. Based on genomic characteristics and sequence divergence, GCRV isolates are generally classified into three genotypes, GCRV-I, GCRV-II, and GCRV-III, which differ considerably in pathogenicity, replication characteristics, and host responses [3, 5]. Quantitative genetic analysis has shown that GCRV resistance in grass carp has low-to-moderate

heritability, indicating exploitable genetic variation and the potential for genetic improvement through selective breeding [6].

The outcome of GCRV infection is influenced not only by viral properties but also by host antiviral responses and genetic variation [3, 7, 8]. Previous studies have shown that grass carp RIG-I and TLR22 respond to GCRV infection and participate in antiviral immune responses [9, 10]. In addition, polymorphisms in the genes encoding Mx2 and RIG-I have been associated with differences in susceptibility or resistance to GCRV [7, 8]. Genome-wide approaches have further facilitated the identification of candidate host factors associated with GCRV resistance. In a previous study from our group, integration of whole-genome resequencing-based GWAS with transcriptomic data highlighted five candidate genes, including *b4galt2*, *kif2c*, *jmjd8*, *selenom*, and *znfx1* [11].

β-1,4-Galactosyltransferase 2 (B4GALT2) belongs to the β-1,4-galactosyltransferase (B4GALT) family, whose members catalyze the transfer of galactose from UDP-galactose to specific acceptor glycans and thereby participate in the biosynthesis and modification of glycoconjugates [12, 13]. Glycosylation is an important modification of proteins and lipids, and increasing evidence indicates that glycan-mediated processes are involved in immune-cell migration, pathogen recognition, innate and adaptive immune responses, immune-cell homeostasis, and inflammation [13, 14]. These functions highlight the potential importance of glycosylation in host defense and host–pathogen interactions. B4GALT2 has also been implicated in diverse cellular and pathological processes, including tumor growth, intestinal inflammation and metabolic regulation, and immune regulation in cancer [15–18]. In particular, B4GALT2 has been linked to immune exclusion in lung adenocarcinoma [17] and to M2 macrophage polarization and immune escape in colorectal cancer [18]. In teleost fish, however, the biological functions of B4galt2 remain poorly characterized. In medaka (*Oryzias latipes*), knockdown of *b4galt2* causes pronounced gastrulation defects, demonstrating an essential role for B4galt2 during medaka gastrulation [19]. Despite these findings, whether and how B4galt2 participates in antiviral responses or virus–host interactions in teleosts remains unclear.

Therefore, the present study aimed to characterize grass carp *b4galt2* and investigate its potential role in GCRV infection. The molecular characteristics, tissue expression patterns, GCRV-induced transcriptional responses, and subcellular localization of B4galt2 were examined, and the effects of *b4galt2* overexpression during infection with two GCRV strains of different genotypes were further evaluated in CIK cells. This study further characterizes B4galt2 in grass carp and supports its potential involvement in GCRV–host interactions.

2. Materials and methods

2.1 Fish, cells, and viruses

Experimental grass carp were obtained from the Grass Carp Genetics and Breeding Center, Ministry of Agriculture and Rural Affairs, Suzhou, Jiangsu Province, China. A separate set of fish from the same

cohort was used in the present study, and samples for *b4galt2* analysis were collected independently. Fish were acclimatized in laboratory tanks with continuous aeration, with the water temperature maintained at 28°C. General fish maintenance conditions were consistent with those described previously [20].

The *Ctenopharyngodon idella* kidney (CIK) cell line, GCRV-JX01 (genotype I), and GCRV-AH528 (genotype II) were maintained in our laboratory. CIK cells were cultured in M199 medium supplemented with fetal bovine serum at 28°C in a humidified incubator with 5% CO_2, as described previously [20].

2.2 RNA extraction, cDNA synthesis, and reverse transcription quantitative PCR

Total RNA was isolated from grass carp tissues or CIK cells using the TRIzol method. RNA concentration and purity were determined using a NanoDrop 2000 spectrophotometer (Thermo Fisher Scientific, USA), and RNA integrity was examined by 1% agarose gel electrophoresis. RNA was reverse-transcribed into cDNA using RT Master Mix for qPCR with gDNA Remover (ABclonal, China), and the synthesized cDNA was stored at − 20°C until further analysis.

Reverse transcription quantitative PCR (RT-qPCR) was performed on a CFX96 Real-Time Detection System (Bio-Rad, USA) using BrightCycle Universal SYBR qPCR Master Mix (ABclonal, China), as described previously [20]. Amplification specificity was evaluated by melt-curve analysis. *EF1α* was used as the internal reference gene, and relative transcript abundance was calculated using the $2^{-\Delta\Delta Ct}$ method [21]. Each biological sample was analyzed in three technical replicates. Primer sequences used in this study are listed in Supplementary Table 1.

2.3 Cloning and bioinformatics analysis of grass carp b4galt2

Gene-specific primers were designed based on the reference sequence of grass carp *b4galt2* retrieved from the NCBI database. The *b4galt2* coding sequence was amplified from grass carp cDNA, and the PCR product was purified and cloned into the pMD™19-T vector (Takara). Positive clones were confirmed by Sanger sequencing at GENEWIZ (Suzhou, China).

The confirmed nucleotide sequence was subsequently subjected to bioinformatics analysis. Sequence similarity was assessed using NCBI BLASTx, while the theoretical molecular mass and isoelectric point (pI) were predicted using ExPASy. Protein domain architecture was predicted using SMART, and multiple sequence alignment of B4galt2 amino acid sequences from grass carp and other species was performed using DNAMAN 8.0. A phylogenetic tree was constructed using the neighbor-joining method in MEGA 7.0 [22]. Protein secondary structure was predicted using Phyre2.2 [23], and three-dimensional structural modeling was performed using SWISS-MODEL. The resulting three-dimensional model was visualized using PyMOL.

2.4 Construction of b4galt2 expression plasmids

Two recombinant expression plasmids were constructed using pcDNA3.1(+) and pCS2-CMVIE94-MCS-EGFP as backbone vectors. Based on the *b4galt2* coding sequence and the corresponding vector sequences, HindIII and BamHI restriction sites were selected, and primers containing homologous arms were designed using the Vazyme single-fragment cloning primer design tool (https://crm.vazyme.com/cetool/singlefragment.html). The *b4galt2* coding sequence was amplified by PCR, and the vectors were linearized with HindIII and BamHI. The purified PCR products were assembled with the corresponding linearized vectors using homologous recombination-based assembly. The assembly products were transformed into DH5α competent cells, and positive clones were screened by colony PCR and confirmed by Sanger sequencing. The pcDNA3.1-*b4galt2* plasmid was used for stable overexpression in CIK cells, whereas pCS2-CMVIE94-MCS-EGFP-*b4galt2* was used for subcellular localization analysis.

2.5 Tissue expression analysis of b4galt2

To characterize the basal tissue expression and temporal expression patterns of *b4galt2* following GCRV challenge, tissue samples were collected from healthy and GCRV-challenged grass carp for subsequent RT-qPCR analysis.

Three healthy grass carp were randomly selected and anesthetized with MS-222. Nine tissues, including brain, mesonephros, head kidney, intestine, liver, spleen, heart, gill, and muscle, were collected, immediately frozen in liquid nitrogen, and stored at − 80°C until RNA extraction.

For the GCRV challenge experiment, healthy grass carp were acclimatized under laboratory conditions for 7 days and then divided into a GCRV-challenged group and a control group. GCRV-AH528 (genotype II), maintained in our laboratory, was used for the in vivo challenge. The median lethal dose (LD50), determined in a preliminary challenge trial, was 2.02×10^4 viral genome copies per fish. Fish in the challenged group received 150 μL of the viral suspension by oral gavage at a dose corresponding to 1 × LD50, whereas control fish received an equal volume of PBS by oral gavage. Tissues collected from unchallenged healthy grass carp before GCRV challenge were used as the day 0 baseline. At 2, 4, 6, 8, 10, 12, and 14 days post-challenge, three fish from the challenged group were randomly sampled and anesthetized with MS-222. Muscle, mesonephros, head kidney, intestine, liver, spleen, heart, and gill tissues were collected and stored at − 80°C until RNA extraction.

2.6 Cell transfection

CIK cells were seeded into 6-well plates and allowed to reach approximately 70–80% confluence before transfection with the corresponding recombinant plasmids using Lipofectamine 2000 (Invitrogen). After 4–6 h, the transfection medium was replaced with fresh complete M199 medium.

2.7 Subcellular localization of B4galt2

For subcellular localization analysis, CIK cells were transfected with pCS2-CMVIE94-MCS-EGFP-*b4galt2*. At 48 h post-transfection, the cells were washed three times with PBS and fixed with 4% paraformaldehyde for 30 min at room temperature. After three washes with PBS, the cells were

permeabilized with 0.2% Triton X-100 for 10 min and washed three times with PBS. The cells were then stained with DAPI for 10 min in the dark. After three additional washes with PBS, fluorescence was observed, and images were acquired using a fluorescence microscope.

2.8 Establishment of stable b4galt2-overexpressing CIK cells

To establish a stable *b4galt2*-overexpressing CIK cell line, CIK cells were transfected with pcDNA3.1-*b4galt2*. At 48 h post-transfection, the cells were cultured in M199 medium containing 100 μg/mL G418 for selection. G418-resistant clones were isolated by limiting dilution, expanded, and evaluated for *b4galt2* mRNA overexpression by RT-qPCR. Parental CIK cells were used as the comparison group in subsequent functional assays.

2.9 GCRV infection and viral transcript analysis

Stable *b4galt2*-overexpressing CIK cells and parental CIK cells were infected with GCRV-JX01 (genotype I) or GCRV-AH528 (genotype II) at a multiplicity of infection (MOI) of 1. After 2 h of viral adsorption at 28°C under 5% CO_2, the virus-containing medium was removed and replaced with M199 medium supplemented with 2% FBS. Cells were collected at the indicated time points after infection, and viral transcript abundance was quantified by RT-qPCR targeting the GCRV-JX01 S9 and GCRV-AH528 S6 genes, respectively.

2.10 Cell viability and plaque formation assays

Cell viability following GCRV infection was assessed using the CCK-8 assay. Stable *b4galt2*-overexpressing CIK cells and parental CIK cells were seeded into 96-well plates at 1×10^4 cells per well and infected with GCRV-JX01 or GCRV-AH528. At 0, 24, and 48 h post-infection, 10 μL of CCK-8 reagent was added to each well, and the cells were incubated for 1 h. Absorbance was measured at 450 nm using a microplate reader.

For the plaque formation assay, stable *b4galt2*-overexpressing CIK cells and parental CIK cells were seeded into 24-well plates at 5×10^4 cells per well and cultured to confluence. GCRV-JX01 was serially diluted tenfold in M199 medium and used to infect the cells. After 2 h of viral adsorption, the inoculum was removed, and the cells were overlaid with 0.3% agarose prepared in M199 maintenance medium. After 48 h of incubation, the cells were fixed with 4% paraformaldehyde for 30 min, after which the agarose overlay was removed and the cells were stained with 0.1% crystal violet for 15 min. Plaque formation was examined to assess GCRV-induced cytopathic effects. Because GCRV-AH528 did not induce discernible cytopathic effects in CIK cells under the experimental conditions, the plaque formation assay was performed only for GCRV-JX01.

2.11 Statistical analysis

Quantitative data are presented as the mean ± standard deviation (SD). Relative expression values from individual biological replicates were log10-transformed before statistical testing. For the basal tissue

expression analysis, differences among tissues were analyzed using one-way repeated-measures ANOVA with the Geisser–Greenhouse correction, followed by Dunnett's multiple-comparisons test using muscle as the reference tissue. For the GCRV challenge experiment, each tissue was analyzed independently using one-way ANOVA followed by Tukey's multiple-comparisons test. Because the gill data showed unequal variances, they were analyzed using Brown–Forsythe and Welch ANOVA followed by Dunnett's T3 multiple-comparisons test. Comparisons between two independent groups were performed using an unpaired two-tailed Student's *t*-test. Two-way ANOVA was used where appropriate for cell-based experiments. $P < 0.05$ was considered statistically significant.

3. Results

3.1 Molecular characterization of grass carp b4galt2

PCR amplification of grass carp cDNA yielded the *b4galt2* coding sequence. The open reading frame (ORF) was 1140 bp in length and encoded a predicted protein of 379 amino acids, with a predicted molecular mass of 43.992 kDa and a theoretical isoelectric point (pI) of 9.56 (Supplementary Fig. 1). Domain analysis revealed an N-terminal galactosyltransferase domain spanning residues 105–238 and a C-terminal galactosyltransferase domain spanning residues 242–319 (Supplementary Fig. 2).

Secondary structure prediction indicated that B4galt2 contained 23% α-helices and 22% β-sheets. A transmembrane helix was also predicted, accounting for approximately 4% of the sequence (Supplementary Fig. 3). Homology modeling generated a three-dimensional model covering 275 residues (73% of the protein sequence), based on the crystal structure of human β-1,4-galactosyltransferase 1 (Supplementary Fig. 4).

3.2 Sequence conservation and phylogenetic analysis of B4galt2

Phylogenetic analysis of B4galt2 homologs from representative vertebrate species showed that grass carp B4galt2 clustered closely with homologs from other teleost species, including crucian carp, common carp, and zebrafish (Supplementary Fig. 5). Teleost B4galt2 homologs clustered together, whereas amphibian, avian, and mammalian homologs were distributed in separate evolutionary branches. Among the species examined, grass carp B4galt2 shared the highest amino acid sequence identity with crucian carp B4galt2 (98.15%), followed by common carp B4galt2 (97.89%) and zebrafish B4galt2 (97.63%). In contrast, lower amino acid sequence identities were observed with human B4GALT2 (68.81%) and chimpanzee B4GALT2 (69.25%).

3.3 Tissue expression of b4galt2 in healthy grass carp

The tissue expression of *b4galt2* was examined in nine tissues from healthy grass carp. *b4galt2* was expressed in all examined tissues, including muscle, mesonephros, head kidney, intestine, liver, spleen, heart, gill, and brain, but its expression levels differed markedly among tissues (Fig. 1). The highest

expression was detected in the brain, where the relative expression level was approximately 55-fold the level in muscle ($P < 0.001$). Relatively high expression was also observed in the heart, at approximately fourfold the level in muscle ($P < 0.01$). In contrast, the liver exhibited the lowest *b4galt2* expression, corresponding to approximately 0.17-fold the level in muscle ($P < 0.05$).

3.4 Expression profiles of b4galt2 following GCRV challenge in grass carp

Relative to the day 0 baseline, *b4galt2* exhibited distinct tissue-specific temporal expression patterns following GCRV challenge (Fig. 2). In muscle and heart, marked changes in *b4galt2* expression were observed as early as day 2, with the highest mean expression detected at this time point. Muscle expression subsequently decreased and showed a second increase at day 12, whereas heart expression declined after day 2 but remained relatively elevated through day 12.

In contrast, the head kidney, mesonephros, liver, and spleen showed delayed expression changes, with the highest mean expression levels detected at day 8. In the mesonephros, *b4galt2* expression increased during the early phase of the challenge, reached its highest mean level at day 8, and remained relatively high at days 10 and 12. Expression in the head kidney, liver, and spleen also increased markedly at day 8 and subsequently declined.

The intestine and gill displayed multiphasic expression patterns. In the intestine, relatively high expression was observed at days 2 and 8. In the gill, high expression levels were detected at days 2, 8, and 10, followed by a reduction in mean expression at later time points. Collectively, these results show dynamic, tissue-specific temporal changes in *b4galt2* expression following GCRV challenge relative to the day 0 baseline.

3.5 Establishment and validation of b4galt2-overexpressing CIK cells

To establish a cellular model for subsequent functional analysis, *b4galt2* expression constructs were introduced into CIK cells. Following transfection with pCS2-CMVIE94-MCS-EGFP-*b4galt2*, EGFP fluorescence was readily observed in CIK cells at 48 h post-transfection (Fig. 3). Stable *b4galt2*-overexpressing CIK cells were subsequently generated by transfection with pcDNA3.1-*b4galt2*, followed by G418 selection and monoclonal expansion. RT-qPCR analysis showed that the relative *b4galt2* mRNA level in the stable cell line was approximately 23-fold that in parental CIK cells (Fig. 4), confirming stable *b4galt2* overexpression at the mRNA level.

3.6 Subcellular localization of B4galt2 in CIK cells

The subcellular distribution of B4galt2 was examined in CIK cells using a B4galt2-EGFP fusion protein. B4galt2-EGFP fluorescence was readily detected, whereas DAPI staining clearly marked the nuclei. In the merged images, the B4galt2-EGFP signal partially overlapped with the DAPI-stained nuclei, while

fluorescence was also observed outside the nuclear regions (Fig. 5). These observations indicate that the B4galt2-EGFP fusion protein was distributed in both the nuclear and cytoplasmic regions of CIK cells.

3.7 Effects of b4galt2 overexpression on GCRV infection in CIK cells

The effects of *b4galt2* overexpression on GCRV infection were evaluated using GCRV-JX01 (genotype I) and GCRV-AH528 (genotype II). Following GCRV-JX01 infection, the S9 transcript level was significantly lower in *b4galt2*-overexpressing cells than in parental CIK cells at 48 h post-infection ($P < 0.0001$) (Fig. 6a). At the same time point, CCK-8–assessed cell viability was significantly higher in *b4galt2*-overexpressing cells than in parental CIK cells ($P < 0.05$) (Fig. 6b). Representative plaque images further showed less extensive plaque formation in *b4galt2*-overexpressing cells following GCRV-JX01 infection (Fig. 6c).

In contrast, following GCRV-AH528 infection, the S6 transcript level was significantly higher in *b4galt2*-overexpressing cells at 24, 48, 72, and 96 h post-infection, with the largest difference between the two cell groups observed at 96 h. No significant difference was detected between the two groups at 120 h post-infection (Fig. 6a). At 48 h post-infection, CCK-8–assessed cell viability was significantly lower in *b4galt2*-overexpressing cells than in parental CIK cells ($P < 0.05$) (Fig. 6b). Because GCRV-AH528 did not induce discernible cytopathic effects in CIK cells under the experimental conditions, plaque assays were performed only for GCRV-JX01. Taken together, the stable *b4galt2*-overexpressing cell line exhibited distinct infection-associated phenotypes relative to parental CIK cells following GCRV-JX01 and GCRV-AH528 infection.

4. Discussion

Our previous GWAS and transcriptomic analysis identified *b4galt2* as one of the candidate genes associated with GCRV resistance [11], but its functional role in GCRV infection remained unclear. The present study therefore systematically characterized grass carp *b4galt2* and investigated its potential involvement in GCRV–host interactions. Collectively, our results show that B4galt2 is highly conserved among teleosts and that *b4galt2* is broadly expressed and shows dynamic temporal expression patterns following GCRV challenge. More importantly, *b4galt2* overexpression exerted distinct effects during infection with GCRV-JX01 and GCRV-AH528, indicating that its effects differ between the two viral strains examined.

The strong conservation of grass carp B4galt2 among teleosts, together with the broad but heterogeneous tissue expression of *b4galt2*, suggests that this glycosyltransferase may have an important physiological role that varies across tissue contexts. β-1,4-galactosyltransferases catalyze the transfer of galactose from UDP-galactose to specific glycan acceptors [24], and B4GALT2 has been shown to contribute to protein-specific N-glycan processing [25]. The biological importance of B4galt2 in fish is further supported by a study in medaka, in which knockdown of *b4galt2* caused pronounced

defects in gastrulation and embryonic morphogenesis [19]. The marked variation in *b4galt2* expression among grass carp tissues may therefore be related to tissue-specific differences in glycosylation-associated cellular processes, as protein glycosylation influences protein stability, trafficking, and cellular function [26]. Particularly noteworthy was the high expression of *b4galt2* in the brain. In B4galt2-deficient mice, reduced levels of the HNK-1 carbohydrate in the brain were accompanied by impaired learning, memory, and motor coordination [27]. Although these findings in mammals cannot be directly extrapolated to grass carp, they provide a relevant biological context for the prominent brain expression observed here. In addition, B4galt2-EGFP fluorescence was observed in the nuclear region as well as in extranuclear regions of CIK cells, indicating a relatively broad intracellular distribution of the fusion protein. Taken together, these observations support a conserved physiological role for B4galt2 while highlighting its tissue-dependent expression and the relatively broad intracellular distribution of the B4galt2-EGFP fusion protein.

Following GCRV challenge, *b4galt2* displayed a pronounced tissue- and time-dependent expression pattern relative to the day 0 baseline. The relatively early changes in muscle and heart; the later increases observed in head kidney, mesonephros, liver, and spleen; and the multiphasic responses in intestine and gill indicate substantial heterogeneity in the regulation of *b4galt2* among tissues. GCRV is distributed unevenly among grass carp tissues; relatively high viral RNA loads have been reported in liver, spleen, kidney, intestine, and muscle at 6–9 days post-infection [4], and GCRV-II has been shown to exhibit broad tissue distribution together with marked changes in immune-related gene expression [2]. At the host level, transcriptomic analysis of spleen tissue from GCRV-resistant and susceptible grass carp further revealed extensive differential gene expression involving immune system and signal transduction pathways [28], indicating that GCRV infection and variation in resistance phenotypes are associated with substantial remodeling of the host transcriptional environment. Such tissue-specific changes may help explain the heterogeneous regulation of *b4galt2* observed here. The known function of B4GALT2 in glycan processing [24, 25] further supports this view, as glycosylation can influence protein stability, trafficking, signaling, and other cellular processes [26]. Comparative transcriptomic analysis of CIK cells infected with different GCRV genotypes also identified dynamic changes in metabolic pathways, including N-glycan biosynthesis [29]. Thus, the observed *b4galt2* expression profiles may reflect infection-associated adjustments in glycosylation-related cellular processes that differ among tissues and stages of infection. Although transcript-level changes alone cannot establish the precise functional role of B4galt2, these results indicate that *b4galt2* regulation is associated with the tissue- and stage-dependent host response to GCRV infection.

At the cellular level, functional analysis in CIK cells revealed that the effect of *b4galt2* overexpression on GCRV infection differed markedly between GCRV-JX01 and GCRV-AH528. During GCRV-JX01 infection, *b4galt2* overexpression was associated with reduced S9 transcript abundance, higher CCK-8–assessed cell viability, and less extensive plaque formation, whereas during GCRV-AH528 infection, S6 transcript abundance was higher in *b4galt2*-overexpressing cells at 24, 48, 72, and 96 h post-infection, and CCK-8–assessed cell viability was lower at 48 h. Because GCRV-AH528 did not induce obvious CPE under the present experimental conditions, the lower CCK-8–assessed cell viability at 48 h should not be

interpreted as direct evidence of increased cell death. Similarly, the S9 and S6 RT-qPCR measurements reflect changes in viral transcript abundance rather than direct measurements of infectious virus production. These contrasting phenotypes indicate that B4galt2 does not exert a uniform antiviral or proviral effect but instead affects infection with GCRV-JX01 and GCRV-AH528 differently. Comparative studies likewise show that genetically distinct GCRVs establish markedly different interactions with the host. In experimentally infected grass carp, GCRV-I and GCRV-II differed substantially in disease progression, mortality, viral RNA accumulation, and the magnitude of host transcriptional responses [3]. Similar genotype-specific differences have been demonstrated in CIK cells, where GCRV-I, GCRV-II, and GCRV-III elicited distinct cytopathic, immune, and metabolic responses; notably, GCRV-II produced no obvious CPE despite inducing a particularly extensive transcriptional response [29]. GCRV-JX01 has also been shown to differ markedly from the genetically distant GCRV-JX02 in its behavior in CIK cells: although both viruses replicated in this cell line, only JX01 induced obvious CPE, and their replication dynamics differed during co-infection [30]. Considerable variation is also evident within GCRV-II itself, as virulent and avirulent isolates produce markedly different hematological and histopathological outcomes in infected grass carp [31]. Further analyses of additional viral transcripts, infectious virus titers, and host antiviral responses such as IFN will help to further clarify the basis of the distinct effects observed during JX01 and AH528 infection. Together, these findings indicate that GCRV infection is shaped by both genotype- and strain-specific virus–host interactions, providing relevant biological context for the contrasting effects of *b4galt2* overexpression observed during JX01 and AH528 infection. Because only one strain representing each genotype was examined in the present study, however, the observed differences should be interpreted specifically in the context of GCRV-JX01 and GCRV-AH528 rather than as a general difference between genotype I and genotype II viruses.

A possible explanation for the contrasting phenotypes observed during JX01 and AH528 infection may involve the glycosylation-related function of B4galt2, although this possibility was not directly examined in the present study. B4GALT2 contributes to protein-specific N-glycan processing [25], suggesting that changes in its expression may selectively affect the glycosylation of particular cellular proteins rather than uniformly altering the cellular glycome. A previous study showed that B4GALT2 interacts with MUC20, promotes its N-glycosylation, and stabilizes the MUC20 protein, thereby influencing downstream biological responses [18]. Such protein-specific effects are potentially relevant to GCRV infection because specific host-cell factors have been shown to influence multiple stages of GCRV infection [32, 33]. For example, the grass carp laminin receptor interacts with the GCRV outer-capsid protein VP5 and contributes to GCRV infection [32], whereas Hsp90 interacts with the GCRV-II outer-capsid protein VP35 and facilitates both viral entry and intracellular proliferation [33]. Evidence for the involvement of host-cell glycans in GCRV infection comes from a study identifying cell-surface heparan sulfate as an attachment receptor for GCRV; enzymatic removal of heparan sulfate markedly reduced viral attachment and infection [34]. Although this finding does not establish a direct link between B4galt2 and heparan sulfate, it shows that the host-cell glycan environment can influence GCRV infection. More broadly, host-cell glycans can function as viral attachment factors or entry receptors, while glycosylation can influence multiple stages of virus–host interactions [35]. Because JX01 and AH528 can elicit different host-cell

responses [3, 29], changes associated with B4galt2 overexpression could potentially influence the two infections through different host-cell processes. Taken together, previous studies support a potential link between host-cell glycosylation and GCRV infection, providing a plausible context for the contrasting phenotypes observed here. However, the present study did not directly assess glycosylation changes, B4galt2 substrates, or GCRV receptors/attachment factors. Therefore, the involvement of glycosylation-related pathways remains a hypothesis that requires direct experimental validation. Further analyses of viral entry, replication kinetics, and host antiviral responses will be needed to determine the basis of the different phenotypes observed during JX01 and AH528 infection.

The present findings do not support classifying B4galt2 as a universal antiviral or proviral factor. Its influence on GCRV infection differed markedly between GCRV-JX01 and GCRV-AH528. This context dependence is consistent with previous studies showing that B4GALT2 participates in distinct biological processes under different cellular and pathological conditions [15–18]. Combined with the previous identification of *b4galt2* as a GCRV resistance-associated candidate gene [11], the overexpression-based functional data presented here support its involvement in GCRV–host interactions. Because the present functional analyses were based on a gain-of-function model, loss-of-function experiments will be required to determine whether endogenous B4galt2 is necessary for the observed phenotypes. In addition, although the S9 and S6 RT-qPCR measurements revealed differences in viral transcript abundance, infectious viral titers were not determined in the present study; therefore, these results should not be interpreted as direct measures of infectious virus production. The contrasting effects observed during JX01 and AH528 infection are also consistent with the possibility that glycosylation-related host processes may contribute to differences in infection outcome. However, parental CIK cells rather than a G418-selected stable empty-vector cell line were used as the comparison group in the functional assays; therefore, potential effects associated with transfection and antibiotic selection cannot be fully excluded.

5. Conclusion

In this study, grass carp *b4galt2* was characterized as a conserved member of the β-1,4-galactosyltransferase family. The gene was broadly expressed across tissues, with the highest expression in the brain, and exhibited tissue- and time-dependent expression changes following GCRV-AH528 challenge. In CIK cells, stable *b4galt2* overexpression was associated with lower S9 transcript abundance, higher CCK-8–assessed cell viability, and less extensive plaque formation during GCRV-JX01 infection. In contrast, higher S6 transcript abundance and lower CCK-8–assessed cell viability were observed during GCRV-AH528 infection at specific time points. These findings provide overexpression-based functional evidence supporting the involvement of B4galt2 in grass carp–GCRV interactions and highlight the contrasting cellular responses associated with its overexpression during infection with the two GCRV strains.

Declarations

Competing Interests

The authors declare no competing interests.

Ethics Approval

All experimental procedures involving grass carp were conducted in accordance with the guidelines for the care and use of laboratory animals and were approved by the Animal Ethics Committee of Shanghai Ocean University (approval no. SHOU-DW-2026-008).

Funding

This work was supported by the National Key R&D Program of China (2023YFD2401602), Jiangxi Province Fishery Seed Industry Joint Research Project (yz2023-06), and China Agriculture Research System (CARS-45-04).

Author Contribution

X.G. contributed to formal analysis, writing the original draft, and reviewing and editing the manuscript. C.Z. contributed to investigation, formal analysis, and methodology. C.T. contributed to methodology. X.C. contributed to investigation. J.L. contributed to project administration and supervision. Y.D. contributed to supervision. Y.S. contributed to project administration, resources, and reviewing and editing the manuscript. S.D. contributed to supervision. All authors read and approved the final manuscript.

Data Availability

The data supporting the findings of this study are presented in the article and its supplementary information. Additional data are available from the corresponding authors upon reasonable request.

References

1. Shen Y, Wang L, Fu J et al (2019) Population structure, demographic history and local adaptation of the grass carp. BMC Genomics 20:467. https://doi.org/10.1186/s12864-019-5872-1
2. Wu M, Li H, Chen X et al (2020) Studies on the clinical symptoms, virus distribution, and mRNA expression of several antiviral immunity-related genes in grass carp after infection with genotype II grass carp reovirus. Arch Virol 165:1599–1609. https://doi.org/10.1007/s00705-020-04654-y
3. He L, Zhang A, Pei Y et al (2017) Differences in responses of grass carp to different types of grass carp reovirus (GCRV) and the mechanism of hemorrhage revealed by transcriptome sequencing.

BMC Genomics 18:452. https://doi.org/10.1186/s12864-017-3824-1

4. Liang H-R, Li Y-G, Zeng W-W et al (2014) Pathogenicity and tissue distribution of grass carp reovirus after intraperitoneal administration. Virol J 11:178. https://doi.org/10.1186/1743-422X-11-178
5. Zeng W, Bergmannc SM, Dong H et al (2021) Identification, Virulence, and Molecular Characterization of a Recombinant Isolate of Grass Carp Reovirus Genotype I. Viruses 13:807. https://doi.org/10.3390/v13050807
6. Tao C, Zhang C, Tang H et al (2026) Estimation of genetic parameters for disease resistance to GCRV in grass carp (*Ctenopharyngodon idella*). Aquac Fish. https://doi.org/10.1016/j.aaf.2026.03.009
7. Wang L, Su J, Peng L et al (2011) Genomic structure of grass carp Mx2 and the association of its polymorphisms with susceptibility/resistance to grass carp reovirus. Mol Immunol 49:359–366. https://doi.org/10.1016/j.molimm.2011.09.010
8. Wan Q, Su J, Chen X et al (2013) Genomic sequence comparison, promoter activity, SNP detection of RIG-I gene and association with resistance/susceptibility to grass carp reovirus in grass carp (*Ctenopharyngodon idella*). Dev Comp Immunol 39:333–342. https://doi.org/10.1016/j.dci.2012.12.004
9. Chen L, Su J, Yang C et al (2012) Functional characterizations of RIG-I to GCRV and viral/bacterial PAMPs in grass carp *Ctenopharyngodon idella*. PLoS ONE 7:e42182. https://doi.org/10.1371/journal.pone.0042182
10. Su J, Heng J, Huang T et al (2012) Identification, mRNA expression and genomic structure of TLR22 and its association with GCRV susceptibility/resistance in grass carp (*Ctenopharyngodon idella*). Dev Comp Immunol 36:450–462. https://doi.org/10.1016/j.dci.2011.08.015
11. Yu C, Jiang Y, Zhang C et al (2024) Whole-genome resequencing of grass carp (*Ctenopharyngodon idella*) for genome-wide association study on GCRV resistance. Aquaculture 592:741243. https://doi.org/10.1016/j.aquaculture.2024.741243
12. Almeida R, Amado M, David L et al (1997) A family of human β4-galactosyltransferases: cloning and expression of two novel UDP-galactose:β-N-acetylglucosamine β1,4-galactosyltransferases, β4Gal-T2 and β4Gal-T3. J Biol Chem 272:31979–31991. https://doi.org/10.1074/jbc.272.51.31979
13. Amado M, Almeida R, Schwientek T, Clausen H (1999) Identification and characterization of large galactosyltransferase gene families: galactosyltransferases for all functions. Biochim Biophys Acta 1473:35–53. https://doi.org/10.1016/S0304-4165(99)00168-3
14. van Kooyk Y, Rabinovich GA (2008) Protein-glycan interactions in the control of innate and adaptive immune responses. Nat Immunol 9:593–601. https://doi.org/10.1038/ni.f.203
15. Tagawa M, Shirane K, Yu L et al (2014) Enhanced expression of the β4-galactosyltransferase 2 gene impairs mammalian tumor growth. Cancer Gene Ther 21:219–227. https://doi.org/10.1038/cgt.2014.21
16. Qu L, Shi K, Xu J et al (2022) Atractylenolide-1 targets SPHK1 and B4GALT2 to regulate intestinal metabolism and flora composition to improve inflammation in mice with colitis. Phytomedicine

98:153945. https://doi.org/10.1016/j.phymed.2022.153945

17. Zhang P, Wang D, Zhou G et al (2025) Novel post-translational modification learning signature reveals B4GALT2 as an immune exclusion regulator in lung adenocarcinoma. J Immunother Cancer 13:e010787. https://doi.org/10.1136/jitc-2024-010787
18. Zhi Y, Zhang Y, Fei H et al (2026) Abnormal glycosylation of MUC20 mediates TAM polarization and promotes immune escape in colorectal cancer. Commun Biol 9:997. https://doi.org/10.1038/s42003-026-10017-1
19. Tonoyama Y, Anzai D, Ikeda A et al (2009) Essential role of beta-1,4-galactosyltransferase 2 during medaka (*Oryzias latipes*) gastrulation. Mech Dev 126:580–594. https://doi.org/10.1016/j.mod.2009.03.004
20. Gao X, Zhang C, Tao C et al (2026) Functional characterization of grass carp (*Ctenopharyngodon idella*) jmjd8 gene in the anti-GCRV immune response. Fish Shellfish Immunol 169:111058. https://doi.org/10.1016/j.fsi.2025.111058
21. Livak KJ, Schmittgen TD (2001) Analysis of Relative Gene Expression Data Using Real-Time Quantitative PCR and the 2 – ΔΔCT Method. Methods 25:402–408. https://doi.org/10.1006/meth.2001.1262
22. Kumar S, Stecher G, Tamura K (2016) MEGA7: Molecular Evolutionary Genetics Analysis Version 7.0 for Bigger Datasets. Mol Biol Evol 33:1870–1874. https://doi.org/10.1093/molbev/msw054
23. Powell HR, Islam SA, David A, Sternberg MJE (2025) Phyre2.2: A Community Resource for Template-based Protein Structure Prediction. J Mol Biol 437:168960. https://doi.org/10.1016/j.jmb.2025.168960
24. Qasba PK, Ramakrishnan B, Boeggeman E (2008) Structure and function of beta – 1,4-galactosyltransferase. Curr Drug Targets 9:292–309. https://doi.org/10.2174/138945008783954943
25. Bydlinski N, Maresch D, Schmieder V et al (2018) The contributions of individual galactosyltransferases to protein specific N-glycan processing in Chinese Hamster Ovary cells. J Biotechnol 282:101–110. https://doi.org/10.1016/j.jbiotec.2018.07.015
26. Schjoldager KT, Narimatsu Y, Joshi HJ, Clausen H (2020) Global view of human protein glycosylation pathways and functions. Nat Rev Mol Cell Biol 21:729–749. https://doi.org/10.1038/s41580-020-00294-x
27. Yoshihara T, Sugihara K, Kizuka Y et al (2009) Learning/memory impairment and reduced expression of the HNK-1 carbohydrate in beta4-galactosyltransferase-II-deficient mice. J Biol Chem 284:12550–12561. https://doi.org/10.1074/jbc.M809188200
28. Yu C, Wu M, Jiang Y et al (2023) Transcriptome Analysis of the Spleen Provides Insight into the Immune Regulation of GCRV Resistance in Grass Carp (*Ctenopharyngodon idella*). Mar Biotechnol 25:557–566. https://doi.org/10.1007/s10126-023-10225-4
29. Kong W, Ding G, Yang P et al (2023) Comparative Transcriptomic Analysis Revealed Potential Differential Mechanisms of Grass Carp Reovirus Pathogenicity. Int J Mol Sci 24:15501.

https://doi.org/10.3390/ijms242115501

30. Wang T, Li J, Lu L (2013) Quantitative in vivo and in vitro characterization of co-infection by two genetically distant grass carp reoviruses. J Gen Virol 94:1301–1309. https://doi.org/10.1099/vir.0.049965-0
31. Tang Y, Zeng W, Wang Y et al (2020) Comparison of the blood parameters and histopathology between grass carp infected with a virulent and avirulent isolates of genotype II grass carp reovirus. Microb Pathog 139:103859. https://doi.org/10.1016/j.micpath.2019.103859
32. Wang H, Yu F, Li J, Lu L (2016) Laminin receptor is an interacting partner for viral outer capsid protein VP5 in grass carp reovirus infection. Virology 490:59–68. https://doi.org/10.1016/j.virol.2016.01.011
33. Jiang L, Liu A, Zhang C et al (2022) Hsp90 Regulates GCRV-II Proliferation by Interacting with VP35 as Its Receptor and Chaperone. J Virol 96:e01175–e01122. https://doi.org/10.1128/jvi.01175-22
34. Wang Q, Wang H, Wang X et al (2025) Cell surface heparan sulfate is an attachment receptor for grass carp reovirus. iScience 28:112033. https://doi.org/10.1016/j.isci.2025.112033
35. Zhai X, Yuan Y, He W-T et al (2024) Evolving roles of glycosylation in the tug-of-war between virus and host. Natl Sci Rev 11:nwae086. https://doi.org/10.1093/nsr/nwae086

Figures

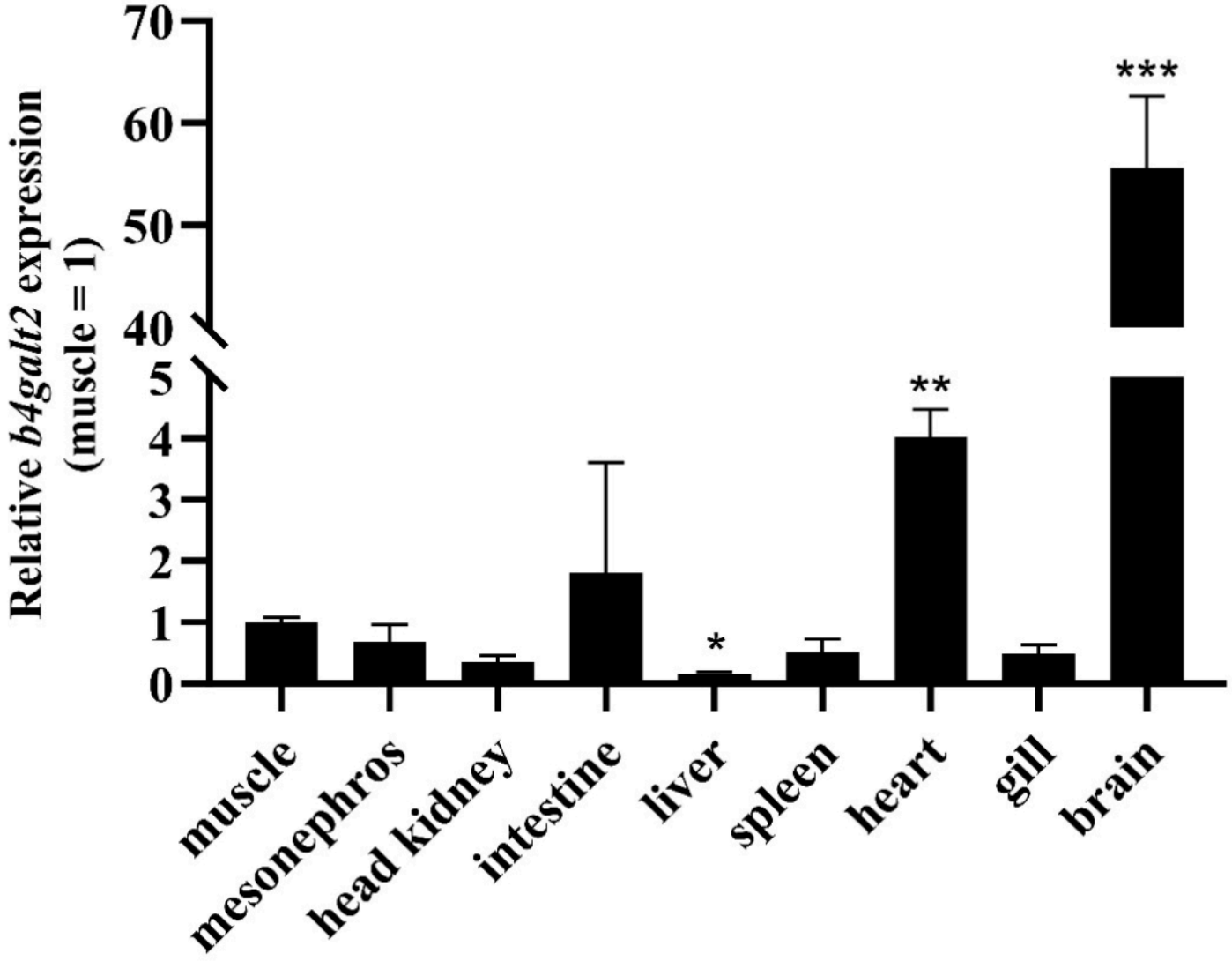

Figure 1

Tissue expression profile of *b4galt2* in healthy grass carp. Relative *b4galt2* mRNA expression was determined by RT-qPCR, with muscle used as the calibrator and set to 1. Data are presented as the mean ± SD (n = 3 fish). Differences among tissues were analyzed using one-way repeated-measures ANOVA with the Geisser–Greenhouse correction, followed by Dunnett's multiple-comparisons test using muscle as the reference tissue. *P< 0.05, **P < 0.01, and ***P < 0.001 compared with muscle. A broken y-axis is used to improve visualization of the large differences in expression levels among tissues.

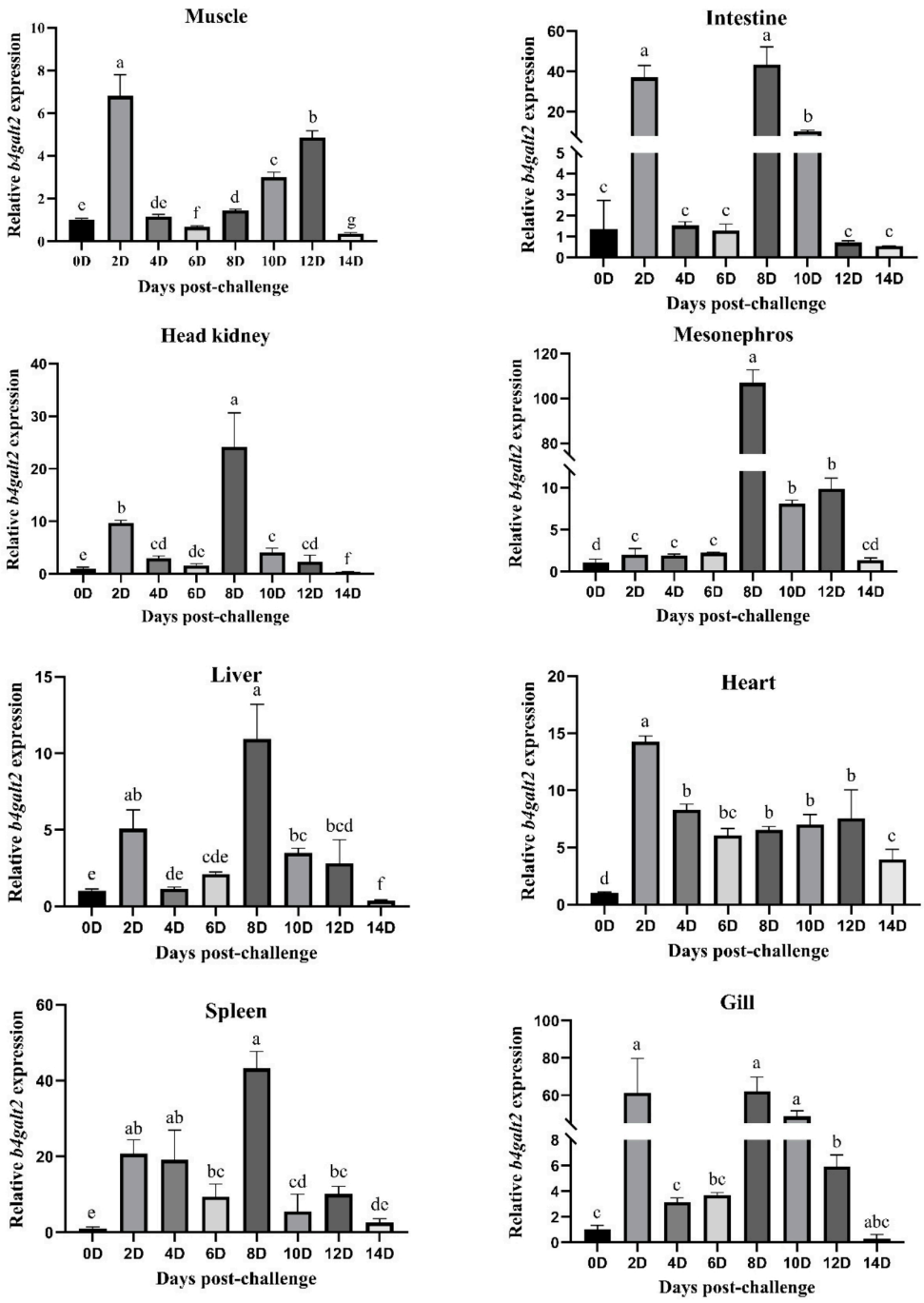

Figure 2

Temporal expression profiles of *b4galt2*in different tissues of grass carp following GCRV challenge. Relative *b4galt2* mRNA expression was determined by RT-qPCR in muscle, intestine, head kidney, mesonephros, liver, heart, spleen, and gill at 0, 2, 4, 6, 8, 10, 12, and 14 days post-challenge. Day 0 represents unchallenged healthy fish sampled before GCRV challenge. Data are presented as the mean ± SD (n = 3 fish per time point). For each tissue, differences among time points were analyzed

independently using one-way ANOVA followed by Tukey's multiple-comparisons test, except for gill, which was analyzed using Brown–Forsythe and Welch ANOVA followed by Dunnett's T3 multiple-comparisons test. Different lowercase letters indicate significant differences among time points within each tissue ($P < 0.05$). Broken y-axes are used for intestine, mesonephros, and gill.

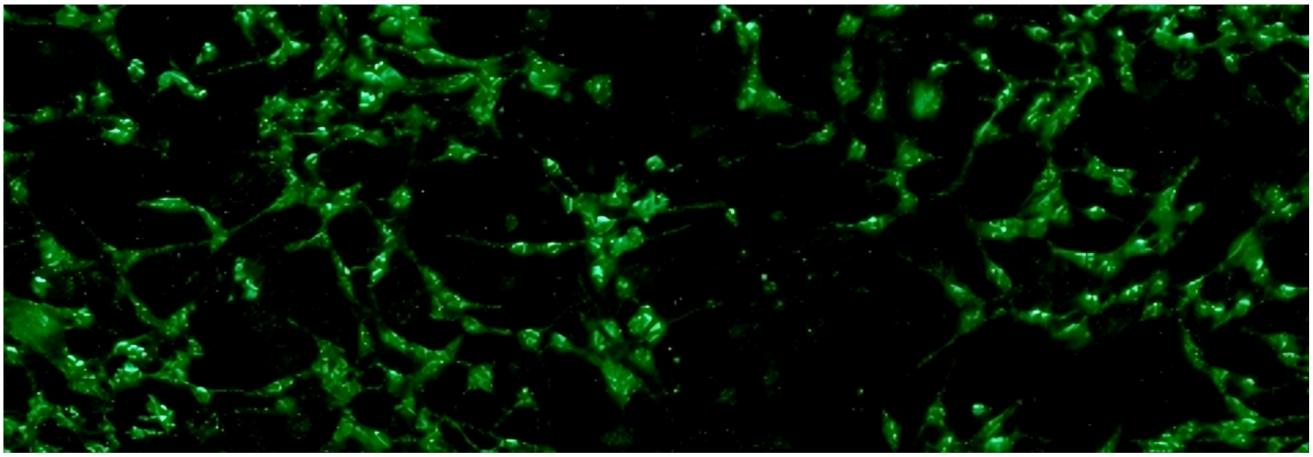

Figure 3

Expression of recombinant B4galt2-EGFP in CIK cells. Representative fluorescence image of CIK cells transfected with the recombinant pCS2-CMVIE94-MCS-EGFP-*b4galt2* plasmid at 48 h post-transfection.

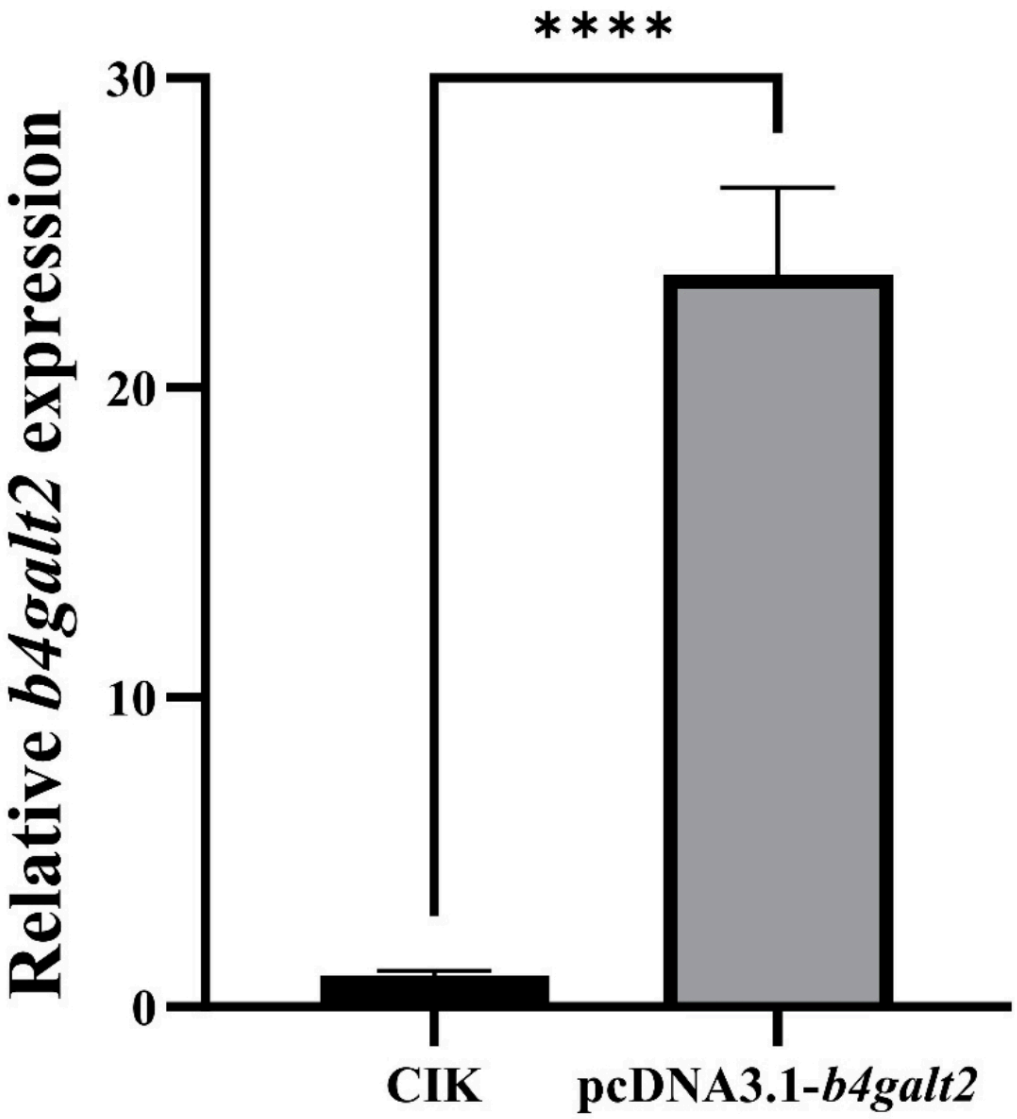

Figure 4

RT-qPCR validation of stable *b4galt2*overexpression in CIK cells. Relative *b4galt2* mRNA expression in parental CIK cells and stable *b4galt2*-overexpressing CIK cells was determined by RT-qPCR. Data are presented as the mean ± SD. ****$P < 0.0001$ compared with parental CIK cells.

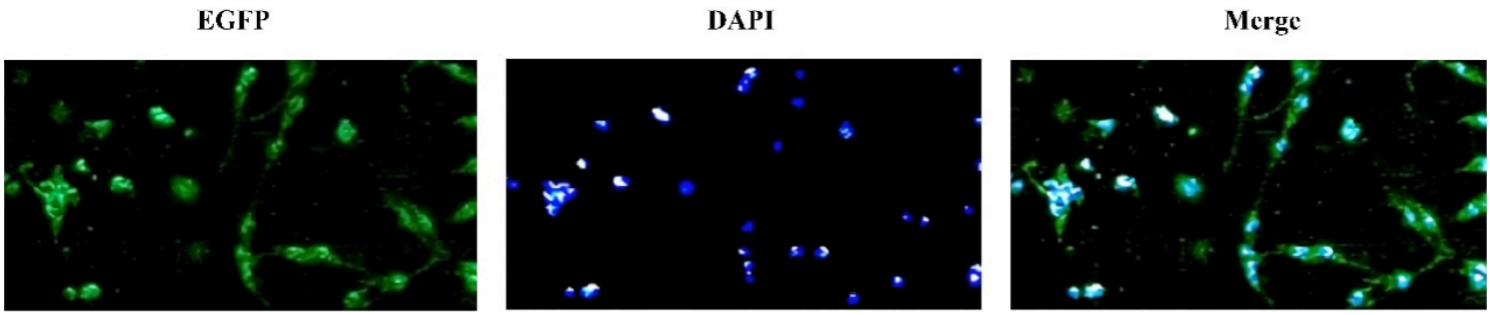

Figure 5

Subcellular distribution of B4galt2-EGFP in CIK cells. Representative fluorescence images showing B4galt2-EGFP fluorescence, DAPI-stained nuclei, and the corresponding merged image.

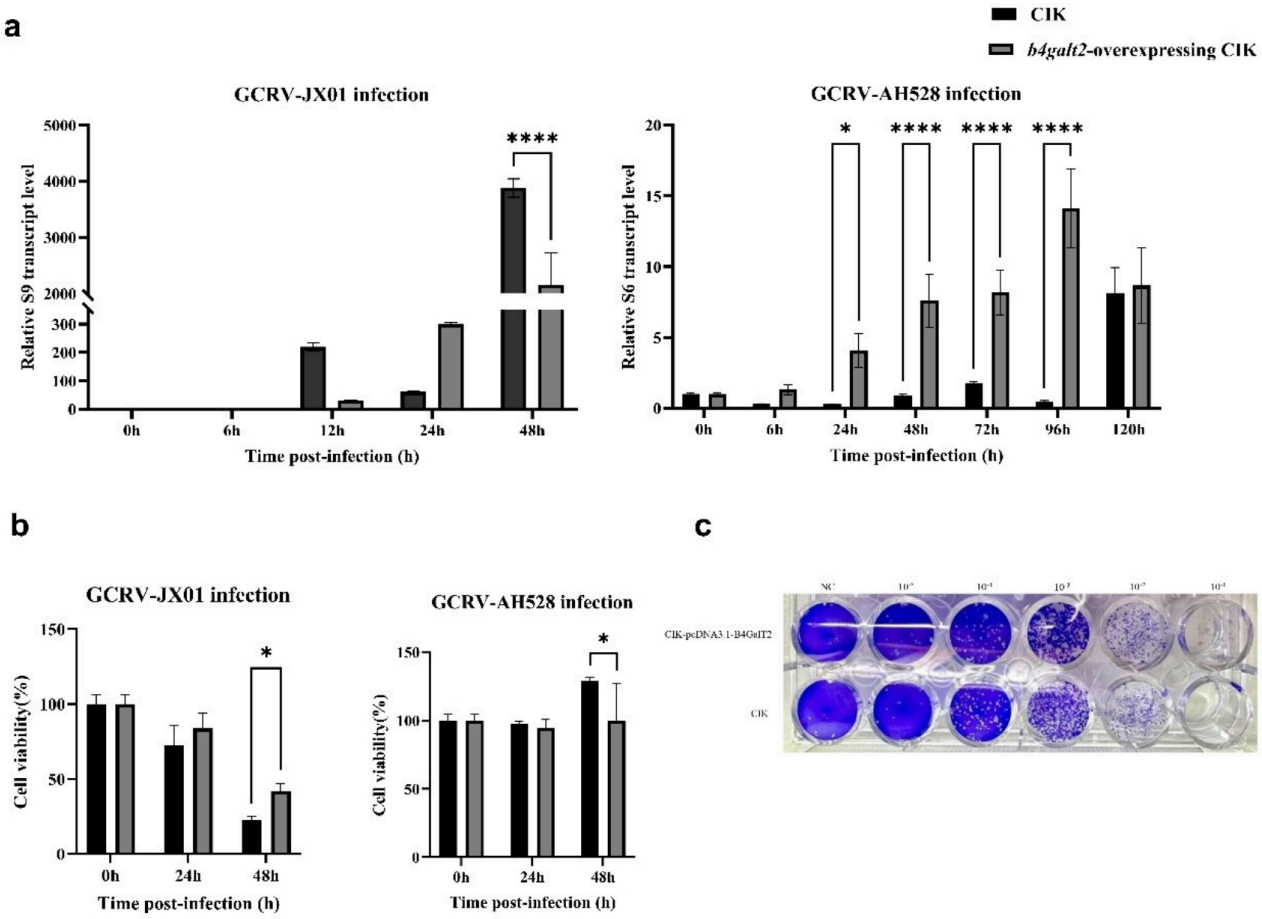

Figure 6

Effects of *b4galt2* overexpression on GCRV infection in CIK cells. (a) Relative S9 and S6 transcript levels in parental CIK cells and *b4galt2*-overexpressing CIK cells following infection with GCRV-JX01 (genotype

I) and GCRV-AH528 (genotype II), respectively. (b) Cell viability of parental CIK cells and *b4galt2*-overexpressing CIK cells following GCRV-JX01 or GCRV-AH528 infection, as assessed by the CCK-8 assay. (c) Representative plaque images of parental CIK cells and *b4galt2*-overexpressing CIK cells following infection with serially diluted GCRV-JX01. Data are presented as the mean ± SD. *P < 0.05 and ****P < 0.0001 compared with parental CIK cells at the corresponding time point.

Supplementary Files

This is a list of supplementary files associated with this preprint. Click to download.

- SupplementaryTab.1.docx
- Supplementarydata.docx